IEEE Access
Multidisciplinary | Rapid Review | Open Access Journal

Received May 27, 2018, accepted June 19, 2018, date of publication June 27, 2018, date of current version July 30, 2018.

Digital Object Identifier 10.1109/ACCESS.2018.2851022

Simulation of Cascading Outages Using a Power-Flow Model Considering Frequency

WENYUN JU, (Student Member, IEEE), KAI SUN, (Senior Member, IEEE), AND RUI YAO, (Member, IEEE)

Department of Electrical Engineering and Computer Science, The University of Tennessee, Knoxville, TN 37996, USA

Corresponding author: Kai Sun (kaisun@utk.edu)

This work was supported in part by the ERC Program of the NSF and DOE under NSF Grant EEC-1041877 and in part by the NSF Grant ECCS-1610025.

ABSTRACT Many steady-state power-flow-based models for cascading outage simulation have not considered frequency, which, however, is an important indicator of generation-load imbalance. This paper proposes a novel steady-state approach for simulating cascading outages. The approach employs a power-flow-based model that considers static power-frequency characteristics of both generators and loads. Thus, the frequency deviation due to active power imbalance can be calculated under cascading outages. Furthermore, a new ac optimal power-flow model considering frequency deviation is proposed to simulate the remedial control when system collapse happens as indicated by the divergence of power flows. Case studies first benchmark the steady-state frequency calculated by the power-flow-based model with time-domain simulation results on a two-area power system, and then test the proposed approach for simulation of cascading outages on the IEEE 39-bus system and an NPCC 48-machine 140-bus power system. The test results are compared with a traditional frequency-independent approach using the conventional power flow and ac optimal power-flow models, and verify that by capturing frequency variations under cascading outages, the proposed approach can more accurately simulate the mechanism of outage propagation.

INDEX TERMS Cascading outages, cascading failures, dynamic load flow, ac optimal power flow considering frequency deviation, frequency, under-frequency load shedding.

NOMENCLATURE

f, f_n	System frequency and nominal frequency
f_d, f_{dmin}, f_{dmax}	Frequency deviation and its lower and upper limits
P_{Di}, P_{D0i}	Active powers of load on bus i at f and f_n
P_{Gi}, P_{G0i}	Active power outputs of bus i at f and f_n
$P_{Gi.min}$, $P_{Gi.max}$	Lower and upper limits of P_{Gi}
D_i	Coefficient of the frequency-sensitive load at bus i
R_i	Speed regulation factor of the generator at bus i
n	Number of buses of the system
m	Number of PQ buses of the system
V_i, $V_{i,min}$, $V_{i,max}$	Voltage magnitude at bus i and its lower and upper limits
θ_i, θ_{ij}	Phase angle at bus i and its difference from bus j
Q_{Gi}	Reactive power output of generator at bus i
Q_{Di}	Reactive power of load at bus i
$Q_{Gi,min}$, $Q_{Gi,max}$	Lower and upper limits of Q_{Gi}
$G_{ij} + \mathrm{j}B_{ij}$	Element of the bus admittance matrix
$\Delta\mathbf{P}_{n\times1}$	Vector of active power mismatches at all buses
$\Delta\mathbf{Q}_{m\times1}$	Vector of reactive power mismatches at PQ buses
ΔP_n	Active power mismatch at the swing bus
$\Delta\mathbf{P}_{(n-1)\times1}$	Vector of active power mismatches at PQ and PV buses
$\Delta\boldsymbol{\theta}_{(n-1)\times1}$	Vector of angle corrections at PQ and PV buses
$\Delta\theta_n$	Angle correction at the swing bus

Δf_d	Correction of frequency deviation
$\mathbf{V}_{m\times m}$	Diagonal matrix made of the V_i's at PQ buses
$\Delta\mathbf{V}_{m\times 1}$	Vector of corrections of V_i's at PQ buses
λ_i	Weighting factor of the load at bus i
S_{ij}, $S_{ij,max}$	Apparent power and transmission capacity of line i-j
$\Delta P_{Di,UFLS}$	Active power load shed by UFLS scheme at bus i
$\Delta Q_{Di,UFLS}$	Reactive power load shed by UFLS scheme at bus i
f_{t}	Frequency threshold triggering UFLS scheme
L_{p}	Percentage of load shed with UFLS scheme
f_1, f_2	Lower and upper limits of normal fequency
$f_{\mathrm{L}}, f_{\mathrm{U}}$	Lower and upper limits of abnormal frequency for restricted time operation
ϕ_0	Unexpected action probability of generator frequency protection

I. INTRODUCTION

Cascading outages have caused major concerns on transmission system reliability [1]–[3]. To simulate cascading outages, several types of models have been proposed: 1) steady-state models, such as the CASCADE model [4], [5], DCSIMSEP [6], [7], Branching process model [8], [9], OPA model [10], improved OPA model [11], AC OPA model [12], TRELSS [13], Manchester model [14], Hidden failure model [15], Interaction graph models [16], [17]; 2) quasi-dynamic models, such as the multi-timescale model in [18]; 3) dynamic models, such as the COSMIC model in [19] and hybrid model in [20] that conduct dynamic time-domain simulation on cascading outages. Although time-domain simulation provides detailed behaviors of the system under outages, its major drawback is the intense time consumption for large power system models. A realistic cascading outage scenario may take tens of minutes to simulate from the initial outages until system collapse. Full time-domain simulation for a large power system over such a long time period will be extremely slow. Also, power system dynamic models used by utility companies or reliability coordinators are mainly for the purpose of short-term transient stability simulation. Those models are seldom validated well for mid-term or long-term simulations like the simulations on cascading outages. Thus, steady-state power-flow based approaches have their advantages to meet the time performance requirements for fast simulation of cascading outages. Also, in most of the duration in cascading outages, the transients following each outage damp out quickly and the system often reach its steady state before the next outage. Therefore, power flow based steady-state or quasi-dynamic models are usually sufficient for the analysis of the overall loss and the mechanism in the propagation of cascading outages [18].

Frequency is an important indicator of the real-time balance between active power of generation and load, especially during cascading outages. Abnormal frequency deviation may trigger under-frequency load shedding (UFLS) [21], [22] and generator frequency protection, causing large amount of loss in generation and load, so it is a significant contributing factor of cascading outages and blackouts [23]. A conventional power flow model assumes the system frequency to be always constant by means of one or multiple swing buses to eliminate any active power imbalance. However, ideal swing buses with infinite capability of power balancing and frequency regulation do not exist in real power systems. In practice, frequency is regulated in a distributed way: first, governors of generators regulate their speeds and active power outputs following their designed regulation strategies; second, frequency-sensitive loads in a system also vary their actual power consumptions with the frequency deviation. Therefore, it is important to consider frequency-related system behaviors and operations in the simulation of cascading outages.

Since the 1970's, efforts have been made to include frequency deviation in power flow models [24]. In [25] published in 1986, a ''dynamic load flow'' (DLF) algorithm in which the unbalanced active power is allocated among all generators with speed controllers was proposed, but such a model cannot obtain the frequency. In [26], the frequency is taken as an unknown variable in DLF calculation. In recent decades, for the purposes of fast simulation or analysis with large power systems, many power flow models considering frequency have been proposed [27]–[37], which mainly incorporate power-frequency characteristics into a power-flow model and consider power-frequency characteristics with loads, speed governors of generators or automatic generation control (AGC). References [28] and [29] consider power-frequency and voltage dependent characteristics of loads and speed governors of generators in power flow models with dispatcher training simulators. Reference [30] considers power-frequency and voltage dependent characteristics with loads, voltage-reactive power characteristic of generators, speed governors of generators in power flow models for security assessment of power systems. References [31]–[33] incorporate power-frequency characteristics of active loads and speed governors of generators into power flow models for risk assessment. Other fields to apply such power-flow models include microgrid control [34], [35] and analyses involving wind generation [36], [37]. Analysis and simulation of cascading outages can also apply such models. References [38] and [39] incorporate frequency deviation into cascading outage simulation based on a DC power flow model, in which frequency deviation is calculated directly from power-frequency characteristics of generators and loads.

This paper proposes a novel steady-state approach for simulation of cascading outages with frequency-related system characteristics and operation actions such as frequency deviation, power-frequency characteristics of generators and loads, UFLS scheme, and generator frequency protection. The contributions of this paper are mainly in these three aspects. First, the proposed approach integrates calculation of frequency deviation into a power flow model like [26]

(called "DLF model" in the rest of the paper since it is developed and inspired from the DLF algorithm in [25]–[33]). Thus, power flow results are able to reflect active power imbalance and address power-frequency characteristics of generators and loads. Second, an AC optimal power flow model considering frequency deviation (for short, AC-OPFf) is proposed, which determines remedial control against system collapse indicated by divergent power flow calculation. Thanks to the consideration of frequency deviation, the DLF and AC-OPFf models enable more credible steady-state simulation on a power system under cascading outages. Third, the proposed approach enables the UFLS scheme and generator frequency protection to be modeled, which is critical but has not yet been addressed by existing steady-state approaches for simulation of cascading outages.

The rest of this paper is organized as follows. Section II presents the proposed simulation approach for cascading outages. It first introduces the DLF model employed in the proposed approach, proposes the novel AC-OPFf model, and then presents the UFLS scheme as well as generator frequency and line protection models used in the proposed approach, and finally compares the procedure of the proposed approach with a conventional approach for simulation of cascading outages. Comprehensive case studies are presented in Section III, which first benchmarks the results of the DLF model with that of time-domain simulation on a two-area system, and then tests the proposed approach using many cascading outage scenarios on the IEEE 39-bus system and NPCC 48-machine, 140-bus system. The simulated cascading outages are analyzed and compared with those from the conventional approach. Finally, Section IV draws the conclusions.

II. PROPOSED SIMULATION APPROACH FOR CASCADING OUTAGES

This section first briefly introduces the DLF model and proposes the AC-OPFf model, which is compared with a conventional AC-OPF model. Then, the section presents the UFLS scheme, as well as the generator and line protection models to be used in the proposed simulation approach.

A. DLF MODEL

The static power-frequency characteristics (SPFCs) of a load at bus i can be approximated by

$$P_{Di} = P_{D0i}(1 + D_i f_d), \quad f_d = f - f_n \tag{1}$$

where f is the system frequency, f_n is the nominal frequency, f_d is the frequency deviation, P_{D0i} is the active power load at f_n, and constant D_i quantifies frequency-sensitivity of the load, showing how active the load changes with frequency deviation.

When active power balance of the system cannot be maintained at the nominal frequency, a frequency deviation exists. The speed governor of a generator at bus i can automatically regulate its steady-state output P_{Gi} according to its regulation factor R_i:

$$P_{Gi} = P_{G0i} - f_d/R_i, \quad P_{Gi,\min} \le P_{Gi} \le P_{Gi,\max} \tag{2}$$

where P_{G0i} is its active power output at f_n, and $P_{Gi,\min}$ and $P_{Gi,\max}$ are the lower and upper limits of active power output.

Consider an n-bus power system having m PQ buses (numbered from 1 to m), $n-m-1$ PV buses (numbered from $m+1$ to $n-1$), and a swing bus with No. n. Calculation of the DLF model targets at eliminating active power mismatches with all n buses and reactive power mismatches with m PQ buses.

$$\Delta P_i = P_{Gi} - P_{Di} - V_i \sum_j V_j(G_{ij}\cos\theta_{ij} + B_{ij}\sin\theta_{ij}) \quad i = 1, \ldots, n \tag{3}$$

$$\Delta Q_i = Q_{Gi} - Q_{Di} - V_i \sum_j V_j(G_{ij}\sin\theta_{ij} - B_{ij}\cos\theta_{ij}) \quad i = 1, \ldots, m \tag{4}$$

where P_{Gi} and P_{Di} are calculated from (1)-(2), Q_{Gi} and Q_{Di} are the reactive power output of generator and reactive power of load at bus i, which are assumed frequency-independent. V_i is the voltage magnitude at bus i, $\theta_{ij} = \theta_i - \theta_j$ is the phase angle difference between buses i and j, and G_{ij} and B_{ij} are the real and imaginary elements in the bus admittance matrix.

Mismatches ΔP_i and ΔQ_i make up an n-vector $\Delta\mathbf{P}_{n\times1}$ for all buses and an m-vector $\Delta\mathbf{Q}_{m\times1}$ for all PQ buses. Note that there are $n+m$ unknown variables including frequency deviation f_d, $n-1$ voltage angles and m voltage magnitudes. The N-R (Newton-Raphson) method can be used to solve (5).

$$\begin{bmatrix} \Delta\mathbf{P}_{n\times1} \\ \Delta\mathbf{Q}_{m\times1} \end{bmatrix} = \begin{bmatrix} \Delta\mathbf{P}_{(n-1)\times1} \\ \Delta P_n \\ \Delta\mathbf{Q}_{m\times1} \end{bmatrix} = \mathbf{J} \begin{bmatrix} \Delta\boldsymbol{\theta}_{(n-1)\times1} \\ \Delta f_d \\ \mathbf{V}^{-1}_{m\times m}\Delta\mathbf{V}_{m\times1} \end{bmatrix} \tag{5}$$

where

$$\mathbf{J} = \begin{bmatrix} \mathbf{J_1}_{(n-1)\times(n-1)} & \dfrac{\partial\Delta\mathbf{P}}{\partial f_d}_{(n-1)\times1} & \mathbf{J_2}_{(n-1)\times m} \\ \dfrac{\partial\Delta P_n}{\partial\boldsymbol{\theta}}_{1\times(n-1)} & \dfrac{\partial\Delta P_n}{\partial f_d} & \mathbf{N}_{1\times m} \\ \mathbf{J_3}_{m\times(n-1)} & \mathbf{0} & \mathbf{J}_{4m\times m} \end{bmatrix}$$

In (5), ΔP_n is the active power mismatch of the swing bus, which will be eliminated unlike that in conventional power flow calculation, $\Delta\mathbf{P}_{(n-1)\times1}$ includes active power mismatches of the other buses, $\Delta\boldsymbol{\theta}_{(n-1)\times1}$ is the vector of angle corrections for all buses except for the swing bus, Δf_d is the correction of system frequency deviation, $\mathbf{V}^{-1}_{m\times m}$ is a diagonal matrix made of the reciprocals of V_i's of m PQ buses, and $\Delta\mathbf{V}_{m\times1}$ is the vector of corrections of V_i's for all PQ buses.

The Jacobian matrix $\mathbf{J}$ is an $(n+m)$-dimensional square matrix containing partial derivatives of the active and reactive power injections with respect to voltage angles, magnitudes and f_d. The elements of $\mathbf{J_1}$, $\mathbf{J_2}$, $\mathbf{J_3}$ and $\mathbf{J_4}$ in the i-th row and j-th column are $\frac{\partial P_i}{\partial\theta_j}$, $\frac{\partial P_i}{\partial V_j}V_j$, $\frac{\partial Q_i}{\partial\theta_j}$, and $\frac{\partial Q_i}{\partial V_j}V_j$, i.e. the same as the corresponding elements in the Jacobian matrix of conventional power flow model. Let the bus angle θ_n of the swing bus

be zero. The other elements of **J** are:

$$\left(\frac{\partial \Delta \mathbf{P}}{\partial f_d}\right)_i = \frac{\partial \Delta P_i}{\partial f_d} = \begin{cases} -P_{D0i}D_i & \text{for PQ buses} \\ -(P_{D0i}D_i + \dfrac{1}{R_i}) & \\ & \text{for PV and swing buses,} \end{cases} \quad i = 1, \ldots, n \tag{6}$$

$$\left(\frac{\partial \Delta P_n}{\partial \boldsymbol{\theta}}\right)_j = \frac{\partial \Delta P_n}{\partial \theta_j} = -V_n V_j (G_{nj} \sin\theta_j + B_{nj} \cos\theta_j), \quad j = 1, \ldots, n-1 \tag{7}$$

$$(\mathbf{N})_j = \frac{\partial \Delta P_n}{\partial V_j} V_j = -V_n V_j (G_{nj} \cos\theta_j - B_{nj} \sin\theta_j), \quad j = 1, \ldots, m \tag{8}$$

Solving the DLF model by the N-R method does not bring much more computational burden than solving a conventional power flow model because only one unknown variable and one equation are added. Note that by considering the active power generation limits, constraint $P_{Gi,\min} \le P_{G0i} - f_d/R_i \le P_{Gi,\max}$ is checked with updated f_d at each iteration of the N-R method. If the constraint is violated, freeze P_{Gi} at the limit.

From (5), the Jacobian matrix **J** with the DLF model has the similar sparsity to that with the conventional power flow model, but has more nonzero elements because of the introduced frequency deviation f_d. **J** with the DLF model has at most $2n + m - 1$ more nonzero elements than that of the conventional power flow model. Consider the total number of elements of the **J** is $(n + m - 1)^2$ for a conventional power flow model or to be $(n + m)^2$ for the DLF model, the ratio of $2n+m-1$ to $(n+m-1)^2$ or $(n+m)^2$ is very small for a large power system. Therefore, the **J** with the DLF model is still quite sparse. For example, the ratio $(2n+m-1)/(n+m-1)^2$ is just equal to 0.007 for the NPCC 48-machine, 140-bus power system.

Finally, there are the following remarks on the DLF model used in the proposed approach:

Remarks:

1) In industry practices, AGC is usually disabled in simulation of cascading outages, so this paper does not consider AGC or secondary frequency regulation in the proposed approach.

2) Reactive power loads are less sensitive to a frequency deviation than active power loads, and are often assumed frequency-independent in [31]–[33], which is also assumed so in this paper.

3) In a conventional power flow model, buses are categorized into PQ buses, PV buses and swing buses. The DLF model may inherit those bus types [24], and the operating quantities on those buses are basically unchanged. For instance, P_{D0i} in (1) and P_{G0i} in (2) respectively correspond to "P" components in PQ and PV buses. In fact, P_{D0i} and P_{G0i} slightly vary with frequency deviation around certain constant values. Strictly speaking, PV and PQ buses in a DLF model only maintain constant voltage magnitudes and reactive power injections. Finally, only one swing bus is needed for the DLF model, which is mainly used as a reference bus for voltage angles.

B. AC-OPFf MODEL

During cascading outage simulation, calculation with the DLF model described by (1)-(8) may diverge, indicating a significantly stressed condition or even system collapse, which can be mitigated by remedial control such as generation redispatch and load shedding. The proposed AC-OPFf model is presented as (9) in Table 1 to model a centralized remedial control scheme. It is compared with a conventional AC-OPF model (10) side by side about the objective function and constraints.

TABLE 1. AC-OPFf and AC-OPF models.

AC-OPFf	AC-OPF
$\min -\sum_i \lambda_i P_{Di}$	$\min -\sum_i \lambda_i P_{Di}$
s.t.	*s.t.*
$\Delta P_i = P_{Gi} - P_{Di}$	$\Delta P_i = P_{Gi} - P_{Di}$
$-V_i \sum_j V_j (G_{ij}\cos\theta_{ij} + B_{ij}\sin\theta_{ij}) = 0$ (9a)	$-V_i \sum_j V_j (G_{ij}\cos\theta_{ij} + B_{ij}\sin\theta_{ij}) = 0$ (10a)
$\Delta Q_i = Q_{Gi} - Q_{Di}$	$\Delta Q_i = Q_{Gi} - Q_{Di}$
$-V_i \sum_j V_j (G_{ij}\sin\theta_{ij} - B_{ij}\cos\theta_{ij}) = 0$ (9b)	$-V_i \sum_j V_j (G_{ij}\sin\theta_{ij} - B_{ij}\cos\theta_{ij}) = 0$ (10b)
$P_{Gi,\min} \le P_{Gi} \le P_{Gi,\max}$ (9c)	$P_{Gi,\min} \le P_{Gi} \le P_{Gi,\max}$ (10c)
$Q_{Gi,\min} \le Q_{Gi} \le Q_{Gi,\max}$ (9d)	$Q_{Gi,\min} \le Q_{Gi} \le Q_{Gi,\max}$ (10d)
$V_{i,\min} \le V_i \le V_{i,\max}$ (9e)	$V_{i,\min} \le V_i \le V_{i,\max}$ (10e)
$-\frac{\pi}{2} \le \theta_i \le \frac{\pi}{2}$ (9f)	$-\frac{\pi}{2} \le \theta_i \le \frac{\pi}{2}$ (10f)
$0 \le P_{Di} \le P_{D0i}$ (9g)	$0 \le P_{Di} \le P_{D0i}$ (10g)
$0 \le Q_{Di} \le Q_{D0i}$ (9h)	$0 \le Q_{Di} \le Q_{D0i}$ (10h)
$\lvert S_{ij} \rvert \le S_{ij,\max}$ (9i)	$\lvert S_{ij} \rvert \le S_{ij,\max}$ (10i)
$Q_{Di}P_{D0i} = \frac{P_{Di}Q_{D0i}}{(1+D_i f_d)}$ (9j)	$Q_{Di}P_{D0i} = P_{Di}Q_{D0i}$ (10j)
$f_{d\min} \le f_d \le f_{d\max}$ (9k)	

In the AC-OPFf model, the objective function is to keep the largest remaining active power load after remedial control. The weighting factor λ_i quantifies the importance of load at bus i. The control variables of AC-OPFf model are P_{Gi}, P_{Di}, Q_{Gi}, Q_{Di}, V_i, θ_i, and f_d, respectively. Here P_{Di} and P_{Gi} are corresponding to equations (1) and (2). First two constraints are power flow equations (9*a* and 9*b*). The rest of constraints are about power generations (9*c* and 9*d*), bus voltage magnitudes and phase angles (9*e* and 9*f*), loads (9*g* and 9*h*), branch flows (9*i*), constant power factors (9*j*), and frequency deviation (9*k*). Note that in the AC-OPFf model, two equality constraints 9(a) and (9j) and three inequality constraints, (9*c*), (9*g*), and (9*k*), involve frequency deviation, so the final calculated frequency deviation may not meet its upper or lower limit in (9k) if a limit in (9*c*) or (9*g*) is met.

In the conventional AC-OPF model, the objective function is also to keep the largest remaining active power load after control. The control variables of AC-OPF model are P_{Gi}, P_{Di}, Q_{Gi}, Q_{Di}, V_i, and θ_i, respectively.

The constraints shown by (10a)-(10j) are similar to those of the AC-OPFf model except that frequency deviation is not considered.

Compared with the AC-OPF model, the AC-OPFf model is more general with consideration of frequency deviation. In fact, the AC-OPF model can be regarded as a special case of the AC-OPFf model with f_d equals zero.

The optimality of the final AC-OPF or AC-OPFf solution depends on what algorithm is used and how much gap to the true global optimum is acceptable. In the simulation of cascading outages, introduction of the AC-OPF or AC-OPFf model does not aim at finding the best control strategy; rather, the mainly purpose is to mimic remedial control by the central control room like the OPF module in OPA models [10]–[12]. Therefore, the AC-OPF or AC-OPFf model aims to find a new feasible power flow solution when system collapse happens. In reality, if the proposed simulation approach is applied by power companies, they may easily replace the AC-OPF or AC-OPFf model by their central remedial control strategies.

C. UNDER-FREQUENCY LOAD SHEDDING SCHEME

The inclusion of frequency deviation in the DLF model also enables UFLS to be simulated when there is a substantial, unacceptable frequency decline. A practical UFLS scheme is typically designed to shed 25-30% of the system load in steps with pre-designated loads in each reliability coordinator region when frequency drops to a low threshold [1]. In addition, more load will be progressively shed if frequency decline continues.

As given in Table 2, this paper adopts an UFLS scheme in the simulation of cascading outages for the proposed approach based on the NERC UFLS reliability standard "PRC-006 NPCC" [40] for NPCC region.

TABLE 2. UFLS scheme of NPCC for different load buses.

100MW or More Load		50 MW or more and less than 100 MW		25 MW or more and less than 50 MW	
f_i (Hz)	L_p(%)	f_i (Hz)	L_p (%)	f_i (Hz)	L_p (%)
59.5	6.5	59.5	14	59.5	28
59.3	6.5	59.1	14	-	-
59.1	6.5	-	-	-	-
58.9	6.5	-	-	-	-

Note: f_i and L_p stand for frequency threshold and percentage of load shed.

In general, shedding active power load $\Delta P_{Di,UFLS}$ also cause curtailment of an amount of reactive power load $\Delta Q_{Di,UFLS}$. If the UFLS scheme is triggered, the percentage of active power load to be shed is determined by frequency thresholds in Table 2. Then the change in reactive power load is calculated by (11) assuming a constant power factor to be maintained.

$$\frac{\Delta Q_{Di,UFLS}}{\Delta P_{Di,UFLS}} = \frac{Q_{Di}}{P_{Di}} \tag{11}$$

D. GENERATOR FREQUENCY AND TRANSMISSION LINE PROTECTIONS

Protective actions with generators and transmission lines may introduce additonal failures and uncertainties to system operations under cascading outages [41], [42]. Utilization of the DLF model enables simulatons of some frequency-related protecitve actions. Generator frequency and transmission line protections are modeled in the proposed approach.

As illustrated by Fig. 1, according to the characteristics of the turbine and power plant auxiliaries, the frequency span of a generator can be divided into three types of ranges [42]: (1) the normal operation range bounded by f_1 and f_2, (2) two restricted time operation ranges outside the normal range bounded by a lower limit f_L and an upper limit f_U, i.e. intervals $[f_L, f_1]$ and $[f_2, f_U]$, and (3) prohibited ranges lower than f_L or higher than f_U.

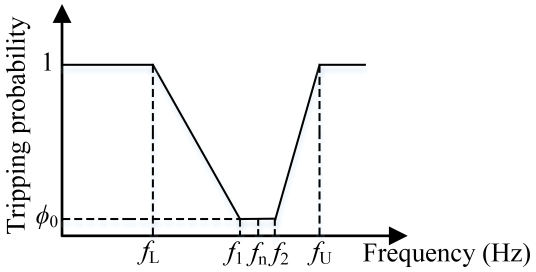

FIGURE 1. Relationship between generator trip probability and frequency.

The tripping probability $\phi(f)$ of generator i as a function of its frequency is shown in (12), where ϕ_0 is the unexpected action probability of generator frequency protection.

$$\phi(f) = \begin{cases} 1 & f < f_L \text{ or } f > f_U \\ \dfrac{(\phi_0 - 1)f + f_1 - \phi_0 f_1}{f - f_L} & f_L \le f \le f_1 \\ \phi_0 & f_1 < f < f_2 \\ \dfrac{(1 - \phi_0)f + \phi_0 f_U - f_2}{f_U - f_2} & f_2 \le f \le f_U \end{cases} \tag{12}$$

The proposed approach models both the UFLS scheme and generator frequency protection, whose relay actions are in different timeframes. For example, the typical time delay of a UFLS scheme is 0.1s for the Eastern Interconnection [40] while the time delays of generator frequency relays vary from 0.1s to several hundreds of seconds depending on the severity of frequency deviation. Accordingly, the proposed simulation approach uses a module shown in Fig. 2 to coordinate the UFLS scheme and generator frequency protection, which performs UFLS for a higher priority than generator frequency protection as long as the criterion of triggering UFLS is satisfied. Only if UFLS is not triggered, generator frequency protection might be triggered at probability $\phi(f)$ defined by (12). This module is embedded into the proposed approach shown by Fig. 3 and represented by the block "UFLS and generator frequency protection module".

With the propagation of cascading outages, a transmission line $i-j$ is overloaded if its apparent power S_{ij} exceeds

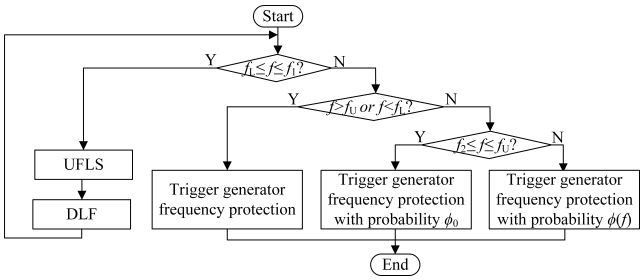

FIGURE 2. UFLS and generator frequency protection module.

transmission capacity $S_{ij,max}$. Each overloaded line is tripped at a probability denoted by β and the probability of tripping the rest of lines is assumed to be $\varepsilon \times \left|\frac{S_{ij}}{S_{ij,\max}}\right|^{\tau}$. Here, ε is a base probability of any unwanted protection operation and should increase with the loading ratio of the line [11].

Remark: The proposed approach is based on a steady-state power flow model, so there is no explicit time evolution information. Unlike time-domain simulation, the tripping sequence and dynamic process on generators are not modeled in detail. In simulation by the proposed approach, once a generator is tripped, it will not be recovered until the end of simulation.

E. SIMULATION PROCEDURE OF THE PROPOSED APPROACH

The proposed approach for the simulation of cascading outages is shown in Fig. 3. For comparison, a conventional approach for simulating cascading outages is shown in Fig. 4, which replaces the DLF and AC-OPFf models by the conventional power flow and AC-OPF models and does not consider the UFLS scheme and generator frequency protection. The block "Parameters and power network initialization" in both Fig. 3 and Fig. 4 performs conventional power flow calculation to obtain a base operating condition with nominal system frequency at 60Hz before the initial line outages are added at the next step.

If the system separates into islands during cascading outages, the bus with the largest active power generation limit in each island can be chosen as the swing bus for that island according to the suggestions from [43]. For the DLF model, the function of the swing bus in each island is not to eliminate active power imbalance by itself; rather, it and other PV buses will compensate the active power imbalance depending on their power-frequency characteristics. The swing bus is then used as a reference bus for voltage angles in each island. If divergence is caused by a large imbalance in real power of any, the AC-OPFf or AC-OPF model will be performed to search for a new solution.

III. CASE STUDIES

This section first uses Kundur's two-area, 4-machine power system [44] to benchmark the frequency calculated by the DLF model with the steady-state frequency obtained from

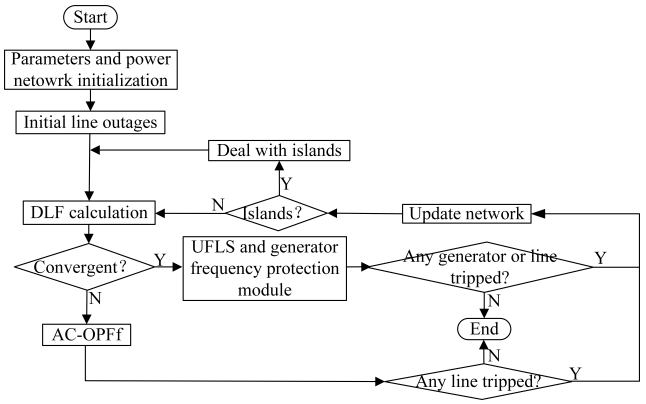

FIGURE 3. Simulation procedure of the proposed approach.

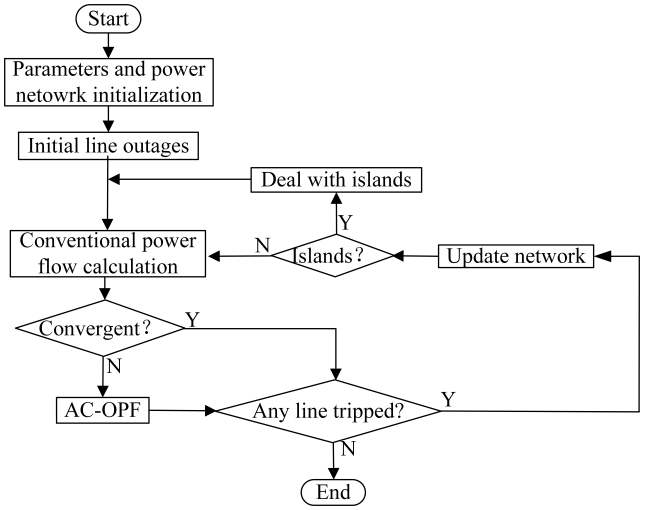

FIGURE 4. Simulation procedure of a conventional approach for comparison.

time-domain simulation. Then, the section compares the simulation results from the proposed and conventional simulation approaches on the IEEE 39-bus power system and NPCC 48-machine, 140-bus power system [45], [46]. Both simulation approaches are implemented in MATLAB. Time-domain simulations are performed by TSAT of Powertech Labs. Parameters in test cases are following.

A. SELECTION OF PARAMETERS

In the DLF model, let $D_i = 1$ pu for all loads in (1), and $R_i = 0.0056$ pu in (2) for all generators, which is based on the system base (100 MVA) after the conversion from the value of R in Table 3 based on the generator base. Let $\lambda_i = 1$ for all loads in AC-OPFf and AC-OPF models. Assume a maximum 0.5 Hz frequency deviation in constraint (9k), i.e. $f_{dmin} = -0.5$ Hz, $f_{dmax} = 0.5$ Hz. The threshold to trigger the UFLS scheme is 59.5 Hz.

For generator frequency protection, set $\phi_0, f_L, f_1, f_n, f_2$, and f_U as 0.002, 57 Hz, 59.5Hz, 60Hz, 60.5Hz, 61.7Hz, respectively in (12). For transmission line protection, let $\beta = 0.999$, $\varepsilon = 0.001$, and $\tau = 10$, the same as [11].

TABLE 3. Parameters for the turbine-governor model.

Parameter	Value	Unit
Speed regulation factor R	0.05	pu
Turbine damping coefficient D_t	0	pu
Main steam control valve max limit V_{max}	1	pu
Main steam control valve min limit V_{min}	0.3	pu
Governor time constant T_1	0.5	s
Steam chest time constant T_2	1.0	s
Reheater time constant T_3	1.0	s

For time-domain simulation on the two-area system as a benchmark for frequency, all generators use the 2nd order classic model equipped with steam turbine-governor model "TGOV1" [47].

For the time-domain simulation on the NPCC power system, 24 generators are represented by a detailed round rotor model "GENROU" with an exciter model "ESDC1A" with PSS/E v32 [48] and the other 24 generators use the classic model. All generators are equipped with the "TGOV1" governor model using the same parameters in Table 3. All loads are modeled as frequency-dependent loads, i.e. "IEELBL" in PSS/E v32 and reactive powers of loads are assumed to be constant.

Transmission capacity limit $S_{ij,max}$ of each line of the IEEE 39-bus system is from the data with MATPOWER 6.0 toolbox. For the NPCC power system, $S_{ij,max}$ of each line is generated by two steps: 1) finding initial limits to make sure no overloading after any N-1 contingency; 2) increasing all limits by 20% to ensure some reliability margin.

B. TESTS ON THE TWO-AREA SYSTEM

The two-area system has loads at buses 7 and 9. To compare steady-state system frequencies from the DLF model and time-domain simulation, three scenarios of load changes are tested: a) shedding the load on bus 7; b) shedding loads on both buses; c) increasing loads on both buses.

From Fig. 5, the steady-state frequencies from the DLF model in all three scenarios match well the time-domain simulation results, which verifies the accuracy of the steady-state frequency calculated from the DLF model.

C. TESTS ON THE IEEE 39-BUS SYSTEM

The following four groups of tests are performed on the IEEE 39-bus system, whose purposes are provided:

1) Verifying the accuracy of steady-state frequency and the convergence characteristics with the DLF model. Two scenarios are designed, i.e. Scenarios 1 and 2.

2) Testing the UFLS and generator frequency protection module and the influence of SPFCs of loads on frequency. One scenario is used, i.e. Scenario 3.

3) Studying the influence of active power generation limits on frequency. Scenario 4 is designed to intentionally make the active power outputs of some generators reach their generation limits after the line outages.

4) Comparing the simulated cascading outages from the proposed approach based on Fig. 3 and conventional approach based on Fig. 4 statistically. Scenarios starting from all N-2 initial outages are considered.

Scenarios 1, 2, 3, and 4 of the above 1)-3) are shown on the IEEE 39-bus system in Fig. 6, distinguished in color.

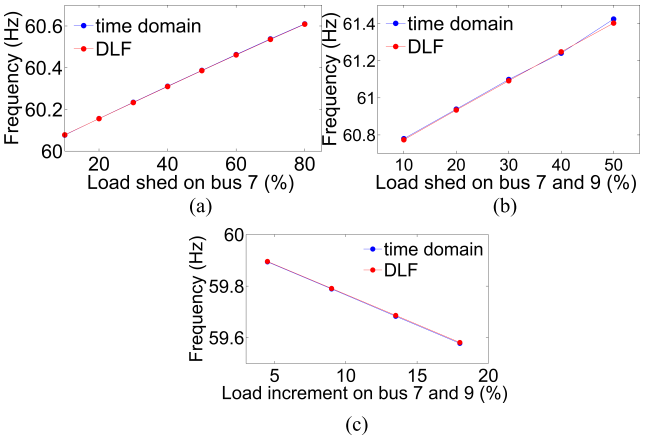

FIGURE 5. Frequency variations from the DLF model and time-domain simulation.

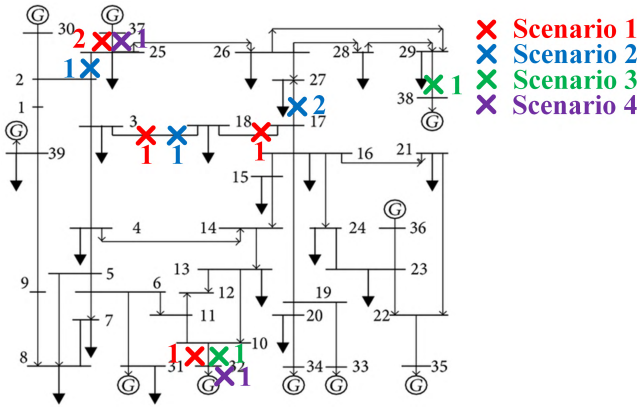

FIGURE 6. Scenarios 1, 2, 3, and 4 on the IEEE 39-bus System (outages are marked with crosses and labeled with stages).

1) VERIFICATION OF STEADY-STATE FREQUENCY

Scenario 1 represents the line outages without causing system separation, and Scenario 2 represents the line outages that cause the system to separate into islands. Those two typical scenarios both introduce major disturbances, i.e. line outages, to cause large power imbalances and significant frequency deviations. The steady-state values of frequencies following the line outages are obtained from both the DLF model and time-domain simulation, and the results are compared.

Scenario 1: Trip line 10-32, line 17-18, and line 3-18 in stage 1 and then trip line 25-37 in stage 2.

In time-domain simulation, two stages are intentionally separated by 100 seconds to make sure that the frequency

can reach its steady-state before the next outage. Frequencies from time-domain and the DLF model for all stages are shown in Fig.7. Only steady-state frequencies are compared. Generator 32 is tripped at stage 1 and then generator 37 is tripped at stage 2. The frequencies calculated by the DLF model for the remaining system at stages 1 and 2 are very close to those from time-domain simulation so as to verify the accuracy of frequency calculated by the DLF model. The slight mismatch for the frequencies between them is because the power flow results of them are not exactly the same.

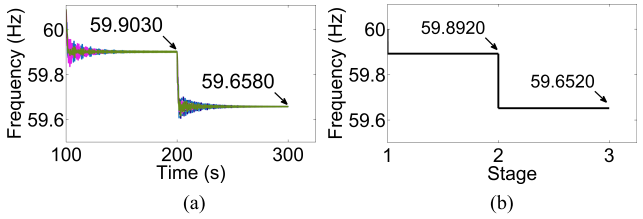

FIGURE 7. Frequency variations of Scenario 1. (a) From time-domain. (b) From the DLF model.

Scenario 2: Trip lines 2-25, 3-18 in stage 1 and trip line 17-27 in stage 2.

The system separates into two islands after line outages in stage 2, including a main island with 8 generators and a smaller island with generators 37 and 38. The steady-state frequencies from the DLF model in stages 1 and 2 are very close to those from simulation as compared in Fig. 8.

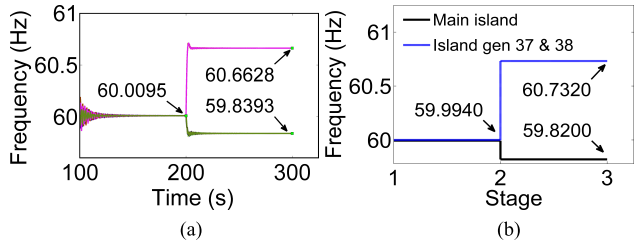

FIGURE 8. Frequency variations of Scenario 2. (a) From time-domain. (b) From the DLF model.

The convergence of N-R method in the DLF model is tested for Scenarios 1 and 2. Fig.9 shows how mismatches of equations in solving the DLF model change with iterations for the two stages of outages. Mismatches drop below the tolerance of 10^{-9}(pu) and power flows converge after 3 or 4 iterations. The mismatch (y-axis) takes the largest value among all ΔP_is and ΔQ_is at each iteration.

Iterations with the N-R method converge at a quadratic rate to the solution when the initial guess is sufficiently close to the solution. For a series $\{x_k\}$ converging to x^* with a quadratic rate, eq. (13) should be satisfied [49], [50].

$$\frac{|x_{k+1}-x^*|}{|x_k-x^*|^2} \le M \quad if\ M > \frac{|h''(x^*)|}{2|h'(x^*)|} \tag{13}$$

For the DLF model or a conventional power flow model, function h in (13) represents (3) and (4) and h' and h'' are

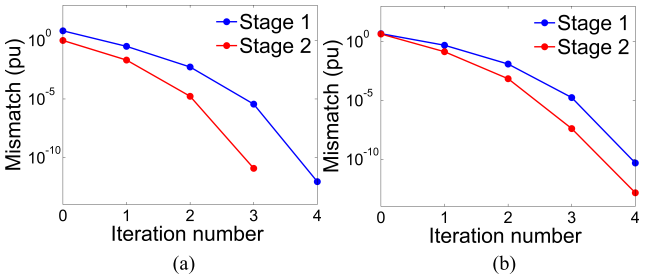

FIGURE 9. Convergence of N-R method with the DLF model. (a) From Scenario 1. (b) From Scenario 2.

the first derivate and second derivate of h. Treat the power flow results at the last iteration on the DLF as the solution x^*. Table 4 calculates $\rho_k = \frac{|x_{k+1}-x^*|}{|x_k-x^*|^2}$ at each iteration step k of the N-R method on the DLF model. From the results, the values of ρ_k for different k's are basically of the same scale, which demonstrates quadratic convergence of the N-R method in solving the DLF model.

TABLE 4. Estimation of convergence rate of DLF calculation.

Scenarios		ρ_k		
		k=0	k=1	k=2
Scenario 1	Stage 1	0.040	0.325	0.380
	Stage 2	0.829	1.353	0.000
Scenario 2	Stage 1	0.027	0.468	0.394
	Stage 2	0.460	0.341	0.413

2) TESTS ON UFLS AND GENERATOR FREQUENCY PROTECTION MODULE AND INFLUENCE OF SPFCS OF LOAD ON FREQUENCY

In the proposed approach for simulation of cascading outages, the UFLS and generator frequency protection module in Fig. 2 will be activated together with some scenarios. Here Scenario 3 tripping lines 32-10 and 38-29 is illustrated.

After tripping lines 32-10 and 38-29, the DLF model gives frequency $f = 59.39$Hz, which falls into the range of 57Hz to 59.5Hz. Then, the UFLS scheme is triggered to shed 384.07MW load and then f increases to 59.55Hz. Since the new frequency f after DLF falls into the range of 59.5Hz to 60.5Hz, generator frequency protections are triggered at a probability of 0.002. Finally, in this scenario, no generator is tripped.

Additionally, the influence of SPFCs of loads on frequency is analyzed in Scenario 3. Fig.10 shows that the larger the parameter D, the smaller is the frequency deviation.

3) INFLUENCE OF ACTIVE POWER GENERATION LIMITS ON FREQUENCY

Active power generation limits are considered in the DLF model. Here, the impact of active power generation limits on frequency is studied on Scenario 4. Table 5 compares active power outputs of generators and system frequencies after tripping lines 10-32 and 25-37 with and without considering active power generation limits, respectively.

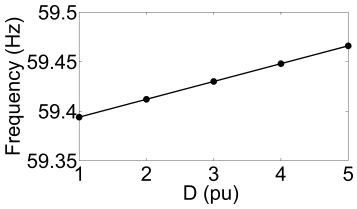

FIGURE 10. Frequency vs *D* of Scenario 3.

TABLE 5. Active power outputs of generators and system frequencies.

Generator	P_{Gmax} (MW)	Without limits		With limits	
		P_G (MW)	f_d (Hz)	P_G (MW)	f_d(Hz)
30	350.00	395.66		350.00	
31	1145.60	507.88		749.74	
33	732.00	777.66		732.00	
34	608.00	653.66		608.00	
35	750.00	795.66	-0.49	750.00	-1.29
36	660.00	705.66		660.00	
38	930.00	975.66		930.00	
39	1100.00	1145.66		1100.00	
32	750.00	-	-	-	-
37	640.00	-	-	-	-

From Table 5, the frequency deviation of -1.29Hz considering active power generation limits is larger than the deviation of -0.49Hz without considering active power generation limits. If some generators reach their active power generation limits, their active power outputs will be fixed at the limits while the other generators such as generator 31 with sufficient margin will continue increasing active power. If active power generation limits are omitted, the frequency deviation may be underestimated.

4) STATISTICAL COMPARISON OF TWO SIMULATION APPROACHES

Some indices evaluating the severity of cascading outages can be used to compare the scenarios of cascading outages generated by the two approaches based on Figs. 3 and 4, such as the number of line outages and amount of load shed. The cascading outage simulations of the two approaches are tested and compared on cascading outage scenarios starting from all N-2 initial outages. Note that the system is N-1 secure, or in other words, it has no overloaded line after any N-1 line outage. Of all the 1035 pairs of cascading outage scenarios derived by the two approaches, the ones which do not propagate beyond the initial outages for both approaches are excluded from comparison. Totally $K = 1028$ scenarios for each approach are compared here.

Define the following two indices to compare the cascading outages simulated by the two approaches.

$$R_{i,path} = \frac{|A_i|}{|B_i|}, \quad R_{i,load} = \frac{Load_{A_i}}{Load_{B_i}}, \quad i = 1, 2, .., K \qquad (14)$$

where A_i and $Load_{Ai}$ are the set of line outages and amount of load shed on scenario i of cascading outages from the conventional approach; B_i and $Load_{Bi}$ are the set of line outages and amount of load shed on scenario i from the proposed approach; $|\cdot|$ represents the number of elements in a set.

Fig. 11(a) shows that for most scenarios, $R_{i,path} < 1$, indicating that line outages propagate more as simulated by the proposed approach than the conventional approach. From Fig. 11(b) and Table 6, the proposed approach tends to have more load shed than the conventional approach due to the consideration of the UFLS scheme and generator frequency protection. It can be inferred that the conventional approach underestimates the extent of outage propagation due to ignoring frequency variations, frequency-related remedial actions and protections. The proposed approach better captures the propagation of outages and losses of load due to frequency-related factors.

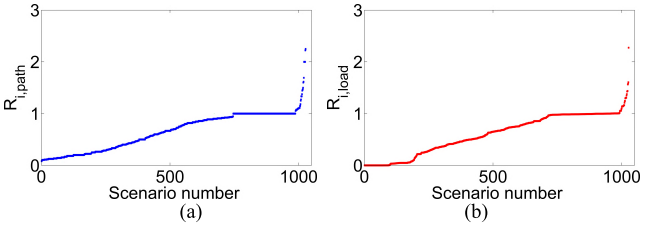

FIGURE 11. Ratios between two approaches (scenario numbers in (a) and (b) are respectively ordered by values of the ratio from small to large). (a) Length of cascading outages. (b) Load shed of cascading outages.

TABLE 6. Statistical comparison of the two approaches with 1028 scenarios.

Approaches	Average No. of line outages	Average amount of load shed (MW)
Conventional	7.76	1848.9
Proposed	12.89	3376.5

Furthermore, the overlaps between the sets of line outages of cascading outages generated by two approaches are evaluated to compare the simulated cascading outage paths. Define the average overlap ratio R_{avg} [19] for the sets of line outages of cascading outages between two approaches as

$$R_{avg} = \frac{1}{K}\sum_{i=1}^{K} R_{i,overlap}, \quad R_{i,overlap} = \frac{|A_i \cap B_i|}{|A_i \cup B_i|} \qquad (15)$$

R_{avg} is 0.61, indicating distinct characteristics of outage propagations simulated by the two approaches.

UFLS is triggered in 255 of the 1028 scenarios. The average, maximum, and minimum amounts of load shed by UFLS scheme are 282.23MW, 599.60MW and 40.85MW, respectively. This study shows that if impacts of frequency deviation and the UFLS scheme are ignored in simulation, the risk of cascading outages will be underestimated.

D. TESTS ON THE NPCC SYSTEM

1) VERIFICATION OF STEADY-STATE FREQUENCY

The steady-state frequency calculated by the DLF model is also verified on the NPCC 48-machine, 140-bus power system.

Two scenarios (numbered Scenarios 5 and 6 below) of cascading outages are selected for verifying the frequencies calculated by the DLF model. The scenarios cause large active power imbalances leading to over- and under-frequency conditions. Note that the purpose of the tests here is only to verify the calculated steady-state frequency, so the AC-OPFf model, the UFLS scheme and generator frequency protection module are deactivated in the two scenarios.

Scenario 5 has two stages of outages as listed in Table 7. The steady-state frequencies obtained from the DLF model and time-domain simulation are compared in Table 8. Scenario 6 has three stages of outages shown by Table 9. The frequencies are compared in Table 10. From the comparisons, the results derived from the DLF model are very close to the benchmarking results, which verifies the accuracy for capturing the steady-state frequency by the DLF model.

TABLE 7. Propagation path of cascading outages in Scenario 5.

Stage	Line Outages
1	130-131, 131-133, 131-135, 131-139
2	124-128, 125-128, 126-128, 127-128, 128-130

TABLE 8. Comparison of steady-state frequencies for Scenario 5.

Approaches	Frequency (Hz)	
	Stage 1	Stage 2
DLF	60.137	60.244
Time-domain	60.147	60.268

TABLE 9. Propagation path of cascading outages in Scenario 6.

Stage	Line Outages
1	85-86, 85-105
2	78-79
3	131-133, 132-133, 133-135

TABLE 10. Comparison of steady-state frequencies for Scenario 6.

Approaches	Frequency (Hz)		
	Stage 1	Stage 2	Stage 3
DLF	59.779	59.622	59.498
Time-domain	59.802	59.649	59.532

Note: three generators are tripped one by one after stages 1, 2 and 3.

2) DETAILED COMPARISON OF TWO SIMULATION APPROACHES

This section conducts detailed comparisons between the proposed approach and conventional approach on two more scenarios numbered 7 and 8. Figs. 12-13 show the outage paths, amounts of load shed and frequency variations of two scenarios.

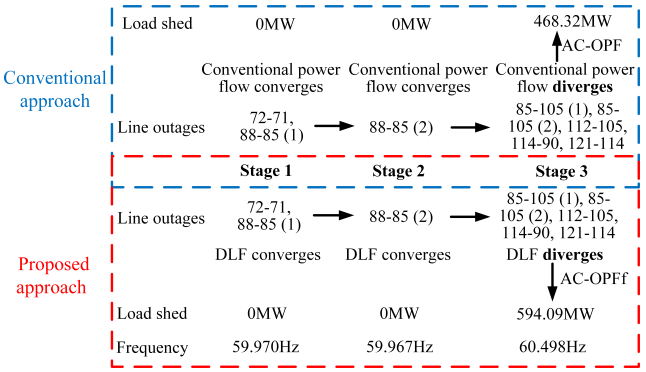

FIGURE 12. Comparison of two approaches on Scenario 7.

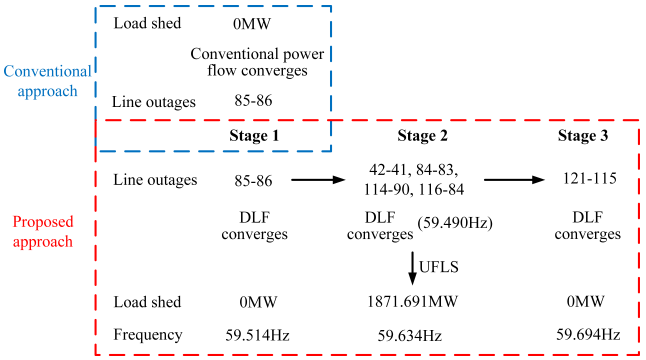

FIGURE 13. Comparison of two approaches on Scenario 8.

For Scenario 7, the outage propagation paths from the same initial outages simulated by two approaches are the same (in Fig. 12), and the frequency deviation is not significant. After stage 2, the frequency only deviates by -0.033Hz. After the line outages in stage 3, power flow calculations by the DLF model and conventional power flow model both diverge, indicating system stress, and then AC-OPF and AC-OPFf are invoked to find new operating points, respectively. The system frequency after AC-OPFf is 60.498 Hz, which is within the normal range, so the UFLS scheme is not triggered. After AC-OPF and AC-OPFf, there are no other lines tripped and outages stop for both approaches. The comparison on Scenario 7 indicates that the two approaches behave similarly with small frequency deviation. However, with the proposed approach, the operators can monitor the variation of system frequency, which is more practical than the conventional approach.

For Scenario 8, the outage propagation paths simulated by two approaches from the same initial outage coincide at the first stage and then differ from stage 2 (Fig. 13). In the simulation with the proposed approach, after line outages at stage 2, the frequency deviation for the remaining system hits -0.51 Hz, so UFLS is triggered to shed load and recover the system frequency to 59.634 Hz. The frequency for the remaining system after stage 3 is 59.694 Hz and UFLS is not

further triggered. The outage propagations and the resulting power flow profiles from the two approaches are relatively close in the first stage and then become distinct from stage 2. This indicates that variations of system frequency cannot be ignored during the propagation of cascading outage, especially for the later stages of outages. Otherwise, the impacts of cascading outages may be significantly underestimated.

3) STATISTICAL COMPARISON OF TWO SIMULATION APPROACHES

A large number of cascading outage scenarios are simulated on the NPCC system using the proposed and conventional approaches to further compare the outage propagation patterns. Each scenario starts from an "N-2" contingency.

For the two approaches, Table 11 compares the average numbers of line outages, the average amounts of load shed by remedial actions, and the average amounts of load shed by the UFLS scheme in 10000 independent scenarios. Cascading outages with the proposed approach tend to propagate more and are more severe than those from the conventional approach. This again indicates the significance of considering frequency variations and frequency-related actions in the simulation of cascading outages.

TABLE 11. Statistical comparison of the two approaches with 10000 Scenarios.

Approaches	Average No. of line outages	Average load shed (MW)	Average load shed by UFLS (MW)
Conventional	8.79	222.45	0
Proposed	14.27	985.02	146.97

The time performances of two approaches are tested on a desktop computer with Intel Core i7-3770K 3.40GHz and 4GB RAM. The total time costs for the same number of scenarios created by two approaches are compared in Table 12. The proposed approach takes about 16% more time than the conventional approach because for a number of scenarios with large frequency deviations, the cascading outages simulated by the proposed approach propagate for more stages and hence require more N-R computations.

TABLE 12. Comparison in time performance.

Number of scenarios	Conventional approach	Proposed approach
10000	14.50 hours	16.78 hours

IV. CONCLUSION

In this paper, a novel steady-state cascading outage simulation approach is proposed, which integrates a DLF model and a novel AC-OPFf model considering frequency deviation. The paper discusses the significance of considering frequency variations in simulation of cascading outages. The proposed approach can accurately capture the steady-state frequency. Also, the proposed AC-OPFf model considering frequency deviation can simulate the control actions against system collapse. Thus, the proposed approach is able to model loss of load due to both frequency insecurity and voltage collapse, and hence can better match practical grid operations than the conventional steady-state approach that ignores the variation of frequency. The proposed approach enables the modeling of frequency related remedial actions and protections such as UFLS scheme and generator frequency protection. The frequency calculated by the DLF model has been benchmarked with time-domain simulation results on both small and large systems. Detailed and statistical comparisons between the proposed and conventional approaches have been conducted to demonstrate the merits of the proposed approach. The proposed approach only focuses on capturing steady-state frequency variations in the simulation of cascading outages and is unable to provide detailed dynamic behaviors of frequency following each disturbance. The future work will integrate this steady-state simulation approach and time-domain simulation for an efficient hybrid simulation approach for cascading outages.

REFERENCES

[1] *Final Report on the August 14, 2003 Blackout in the United States and Canada: Causes and Recommendations*, U.S.-Canada. Power System Outage Task Force, Apr. 2004.

[2] A. Atputharajah and T. K. Saha, "Power system blackouts—Literature review," in *Proc. 4th Int. Conf. Ind. Inf. Syst.*, Sri Lanka, 2009, pp. 460–465.

[3] M. Vaiman *et al.*, "Risk assessment of cascading outages: Methodologies and challenges," *IEEE Trans. Power Syst.*, vol. 27, no. 2, pp. 631–641, May 2012.

[4] B. A. Carreras, V. E. Lynch, I. Dobson, and D. E. Newman, "Dynamical and probabilistic approaches to the study of blackout vulnerability of the power transmission grid," in *Proc. 37th HICSS*, Big Island, HI, USA, 2004.

[5] I. Dobson, B. A. Carreras, and D. E. Newman, "A loading-dependent model of probabilistic cascading failure," *Probability Eng. Inf. Sci.*, vol. 19, no. 1, pp. 15–32, 2005.

[6] M. J. Eppstein and P. D. H. Hines, "A 'Random Chemistry' algorithm for identifying collections multiple contingencies that initiate cascading failure," *IEEE Trans. Power Syst.*, vol. 27, no. 3, pp. 1698–1705, Aug. 2012.

[7] P. Rezaei, P. D. H. Hines, and M. J. Eppstein, "Estimating cascading failure risk with random chemistry," *IEEE Trans. Power Syst.*, vol. 30, no. 5, pp. 2726–2735, Sep. 2015.

[8] I. Dobson, J. Kim, and K. R. Wierzbicki, "Testing branching process estimators of cascading failure with data from a simulation of transmission line outages," *Risk Anal.*, vol. 30, no. 4, pp. 650–662, Apr. 2010.

[9] J. Qi, W. Ju, and K. Sun, "Estimating the propagation of interdependent cascading outages with multi-type branching processes," *IEEE Trans. Power Syst.*, vol. 32, no. 2, pp. 1212–1223, Mar. 2017.

[10] I. Dobson, B. A. Carreras, V. E. Lynch, and D. E. Newman, "An initial model for complex dynamics in electric power system blackouts," in *Proc. 34th HICSS*, Maui, HI, USA, 2001, pp. 710–718.

[11] S. Mei, F. He, X. Zhang, S. Wu, and G. Wang, "An improved OPA model and blackout risk assessment," *IEEE Trans. Power Syst.*, vol. 24, no. 2, pp. 814–823, May 2009.

[12] S. Mei, Y. Ni, G. Wang, and S. Wu, "A study of self-organized criticality of power system under cascading failures based on AC-OPF with voltage stability margin," *IEEE Trans. Power Syst.*, vol. 23, no. 4, pp. 1719–1726, Nov. 2008.

[13] M. Bhavaraju and N. Nour, "TRELSS: A computer program for transmission reliability evaluation of large-scale systems," Electr. Power Res. Inst., Palo Alto, CA, USA, Tech. Rep. EPRI-TR-100566, 1992.

[14] D. P. Nedic, "Criticality in a cascading failure blackout model," *Int. J. Elect. Power Energy Syst.*, vol. 28, no. 9, pp. 627–633, 2006.

[15] J. Chen, J. S. Thorp, and I. Dobson, "Cascading dynamics and mitigation assessment in power system disturbances via a hidden failure model," *Int. J. Elect. Power Energy Syst.*, vol. 27, no. 4, pp. 318–326, May 2005.

[16] J. Qi, K. Sun, and S. Mei, "An interaction model for simulation and mitigation of cascading failures," *IEEE Trans. Power Syst.*, vol. 30, no. 2, pp. 804–819, Mar. 2015.
[17] W. Ju, K. Sun, and J. Qi, "Multi-layer interaction graph for analysis and mitigation of cascading outages," *IEEE J. Emerg. Sel. Topics Circuits Syst.*, vol. 7, no. 2, pp. 239–249, Jun. 2017.
[18] R. Yao, S. Huang, K. Sun, F. Liu, X. Zhang, and S. Mei, "A multi-timescale quasi-dynamic model for simulation of cascading outages," *IEEE Trans. Power Syst.*, vol. 31, no. 4, pp. 3189–3201, Jul. 2016.
[19] J. Song, E. Cotilla-Sanchez, G. Ghanavati, and P. D. H. Hines, "Dynamic modeling of cascading failure in power systems," *IEEE Trans. Power Syst.*, vol. 31, no. 2, pp. 1360–1368, Mar. 2016.
[20] P. Henneaux, P.-E. Labeau, J.-C. Maun, and L. Haarla, "A two-level probabilistic risk assessment of cascading outages," *IEEE Trans. Power Syst.*, vol. 31, no. 3, pp. 2393–2403, May 2016.
[21] Q. Shi, F. Li, Q. Hu, and Z. Wang, "Dynamic demand control for system frequency regulation: Concept review, algorithm comparison, and future vision," *Electr. Power Syst. Res.*, vol. 154, pp. 75–87, Jan. 2018.
[22] H. Pulgar-Painemal, Y. Wang, and H. Silva-Saravia, "On inertia distribution, inter-area oscillations and location of electronically-interfaced resources," *IEEE Trans. Power Syst.*, vol. 33, no. 1, pp. 995–1003, Jan. 2018.
[23] G. Andersson *et al.*, "Causes of the 2003 major grid blackouts in North America and Europe, and recommended means to improve system dynamic performance," *IEEE Trans. Power Syst.*, vol. 20, no. 4, pp. 1922–1928, Nov. 2005.
[24] M. Okamura *et al.*, "A new power flow model and solution method—Including load and generator characteristics and effects of system control devices," *IEEE Trans. Power App. Syst.*, vol. PAS-94, no. 3, pp. 1042–1050, Nov. 1975.
[25] R. Ramanathan, H. Ramchandani, and S. A. Sackett, "Dynamic load flow technique for power system simulators," *IEEE Trans. Power Syst.*, vol. PWRS-1, no. 3, pp. 25–30, Aug. 1986.
[26] I. Roytelman and S. M. Shahidehpour, "A comprehensive long term dynamic simulation for power system recovery," *IEEE Trans. Power Syst.*, vol. 9, no. 3, pp. 1427–1433, Aug. 1994.
[27] M. S. Ćalović, and V. C. Strezoski, "Calculation of steady-state load flows incorporating system control effects and consumer self-regulation characteristics," *Int. J. Elect. Power Energy Syst.*, vol. 3, pp. 65–74, Apr. 1981.
[28] Y. Ping, "A fast load flow model for a dispatcher training simulator considering frequency deviation effects," *Elect. Power Energy Syst.*, vol. 20, no. 3, pp. 177–182, 1998.
[29] Y. Q. Hai, X. Wei, and W. X. Fen, "The improvement of dynamic power flow calculation in dispatcher training simulator," *Autom. Elect. Power Syst.*, vol. 23, no. 23, pp. 20–22, 1999.
[30] D. P. Popović, "An effecient methodology for steady-state security assessment of power systems," *Int. J. Elect. Power Energy Syst.*, vol. 10, no. 2, pp. 110–116, 1988.
[31] Y. Duan and B. Zhang, "Security risk assessment using fast probabilistic power flow considering static power-frequency characteristics of power systems," *Int. J. Elect. Power Energy Syst.*, vol. 60, pp. 53–58, Sep. 2014.
[32] X. Ye, Z. Wuzhi, S. Xinli, and C. Lin, "Power system risk assessment method based on dynamic power flow," in *Proc. Int. Conf. Probabilistic Methods Appl. Power Syst.*, Oct. 2016, pp. 1–4.
[33] P. Bei *et al.*, "Probabilistic dynamic load flow algorithm considering static security risk of the power system," in *Proc. Int. Conf. Electr. Utility Deregulation Restruct. Power Technol.*, Changsha, China, 2015.
[34] Y. H. Liu, Z. Q. Wu, S. J. Lin, and N. P. Brandon, "Application of the power flow calculation method to islanding microgrids," in *Proc. Int. Conf. Sustain. Power Gener. Supply*, Nanjing, China, 2009, pp. 1–6.
[35] L. Rese, A. S. Costa, and A. S. E. Silva, "A modified load flow algorithm for microgrids operating in islanded mode," in *Proc. IEEE PES Conf. Innov. Smart Grid Technol.*, Sao Paulo, Brazil, Apr. 2013, pp. 1–7.
[36] Y. Duan and B. Zhang, "An improved fast decoupled power flow model considering static power–frequency characteristic of power systems with large-scale wind power," *IEEE Trans. Elect. Electron. Eng.*, vol. 9, no. 2, pp. 151–157, Mar. 2014.
[37] S. Li, W. Zhang, and Z. Wang, "Improved dynamic power flow model with DFIGs participating in frequency regulation," *IEEE Trans. Elect. Energy Syst.*, vol. 27, no. 12, pp. 1–13, Dec. 2017.
[38] O. A. Mousavi, R. Cherkaoui, and M. Bozorg, "Blackouts risk evaluation by Monte Carlo simulation regarding cascading outages and system frequency deviation," *Electr. Power Syst. Res.*, vol. 89, pp. 157–164, Aug. 2012.
[39] O. A. Mousavi, M. Bozorg, R. Cherkaoui, and M. Paolone, "Inter-area frequency control reserve assessment regarding dynamics of cascading outages and blackouts," *Electr. Power Syst. Res.*, vol. 107, pp. 144–152, Feb. 2014.
[40] *Automatic Underfrequency Load Shedding*, Standard PRC-006-NPCC-1, Feb. 2012. [Online]. Available: http://www.nerc.com/files/PRC-006-NPCC-1.pdf
[41] S. Imai and T. Yasuda, "UFLS program to ensure stable island operation," in *Proc. IEEE PES Power Syst. Conf. Expo.*, Oct. 2004, pp. 283–288.
[42] *IEEE Guide for Abnormal Frequency Protection for Power Generating Plants*, Standard C37.106-2003, 2004.
[43] A. G. Exposito, J. L. M. Ramos, and J. R. Santos, "Slack bus selection to minimize the system power imbalance in load-flow studies," *IEEE Trans. Power Syst.*, vol. 19, no. 2, pp. 987–995, May 2004.
[44] P. Kundur, *Power System Stability and Control*. New York, NY, USA: McGraw-Hill, 1994.
[45] W. Ju, J. Qi, and K. Sun, "Simulation and analysis of cascading failures on an NPCC power system test bed," in *Proc. IEEE Power Energy Soc. General Meeting*, Denver, CO, USA, Jul. 2015, pp. 1–5.
[46] M. Variani, S. Wang, and K. Tomsovic, "Study of flatness-based automatic generation control approach on an NPCC system model," in *Proc. IEEE Power Energy Soc. General Meeting*, Denver, CO, USA, Jul. 2015, pp. 1–5.
[47] P. M. Anderson and M. Mirheydar, "A low-order system frequency response model," *IEEE Trans. Power Syst.*, vol. 5, no. 3, pp. 720–729, Aug. 1990.
[48] *PSS/E V32 User Manual*, Siemens Power Transmiss. & Distrib. Inc., Heber Springs, AR, USA, Dec. 2007.
[49] A. Melman, "Geometry and convergence of Euler's and Halley's methods," *SIAM Rev.*, vol. 39, no. 4, pp. 728–735, 1997.
[50] I. Shames, F. Farokhi, and M. Cantoni, "Guaranteed maximum power point tracking by scalar iterations with quadratic convergence rate," in *Proc. IEEE 55th Conf. Decis. Control*, Las Vegas, NV, USA, Dec. 2016, pp. 2840–2845.

WENYUN JU (S'15) received the B.E. degree in electrical information from Sichuan University, Chengdu, China, in 2010, and the M.Sc. degree in electrical and electronic engineering from the Huazhong University of Science and Technology, Wuhan, China, in 2013. He is currently pursuing the Ph.D. degree with the Department of EECS, The University of Tennessee, Knoxville, TN, USA. His research interests include cascading outages and vulnerability assessment of power grids.

KAI SUN (M'06–SM'13) received the B.S. degree in automation and the Ph.D. degree in control science and engineering from Tsinghua University, Beijing, China, in 1999 and 2004, respectively. He was a Project Manager in grid operations and planning with EPRI, Palo Alto, CA, USA, from 2007 to 2012. He is currently an Associate Professor with the Department of EECS, The University of Tennessee, Knoxville, TN, USA. His research interests include stability, dynamics and control of power grids, and other complex systems. Prof. Sun serves on the Editorial Boards of the IEEE TRANSACTIONS ON SMART GRID, the IEEE ACCESS, and *IET Generation, Transmission and Distribution*.

RUI YAO (S'12–M'17) received the B.S. (Hons.) and Ph.D. degrees in electrical engineering from Tsinghua University, Beijing, China, in 2011 and 2016, respectively. He is currently a Postdoctoral Research Associate with the Department of Electrical Engineering and Computer Science, The University of Tennessee, Knoxville, TN, USA.